Bioinspired micro-composite structure

L. Chen and R. Ballarini[a)]
Department of Civil Engineering, Case Western Reserve University, Cleveland, Ohio 44106-7201
H. Kahn and A.H. Heuer
Department of Materials Science and Engineering, Case Western Reserve University, Cleveland, Ohio 44106

(Received 4 May 2006; accepted 13 September 2006)

This paper presents the design, fabrication, and mechanical testing of a bioinspired composite structure with characteristic dimensions on the order of tens of microns. The microarchitecture, designed and fabricated using microelectromechanical systems (MEMS) technology, involves two distinct length scales and represents the first attempt at mimicking the crossed-lamellar microstructure of molluscan shells such as the giant Queen conch, *Strombus gigas*, which contains features with dimensions spanning five distinct length scales. The displacement control capabilities of a nanoindenter enabled the observation of the graceful failure of the micro-composite under three point bending and, in turn, the measurement of its post-peak load–displacement response and work of fracture.

I. INTRODUCTION

Studies performed on natural brittle materials suggest a pervasive theme, namely that nature makes structures, not materials, and that these structures are often laminated. The structures created by organisms, although made from rather mundane materials, show impressive properties, which furthermore are very well suited for the intended function (structure/function/performance correlations have been assumed due to natural selection). The diversity of microstructure in molluscan shells testifies to the flexibility of this approach. It would be desirable if materials scientists developed techniques to produce structures, as opposed to materials, and undertook such developments in collaboration with mechanical designers. Study and careful analysis of naturally occurring composites—an aspect of the so-called biomimetic or bioinspired approach—can provide much insight for the design of new, improved materials, particularly composites composed of a large volume fraction of a brittle constituent. Laminated structures composed of mostly brittle constituents offer promise in a wide range of applications, including hot section components in aircraft engines, pavement material for airfields and roads, and electronic packaging.

Exploration of the mechanical behavior of a diverse array of microstructural designs through fabrication and mechanical testing is economically prohibitive. Therefore, the development of bioinspired structural designs will undoubtedly rely on multiscale computational tools whose predictions will be assessed through limited numbers of carefully designed experiments. Microelectromechanical systems (MEMS) technology offers promise for prototyping structural designs of laminated composites and can provide data to assess the predictive capabilities of the computational models because it enables economical fabrication of very large numbers of specimens on a single chip; testing using commercially available nanoindenters and probe stations is then straightforward. For the micro-composite described in this paper, as many as 576 specimens were fabricated on each chip.

The inspiration for the micro-composite structure described in this paper comes from previous studies of the microarchitecture of molluscan shells,[1–3] which are exquisitely designed biocomposites (biological ceramics) consisting of calcitic or aragonitic $CaCO_3$ and a small quantity of organic components (the non-mineral portion of mineralized tissue is referred to as the matrix in biological jargon). They are common examples of very heavily mineralized hard tissue, the organic components comprising as little as 1% of the shell volume. Compared with engineered ceramics or nonbiogenic (mineral) calcium carbonate, mollusk shells exhibit an extraordinary work of fracture, several orders of magnitude higher than ceramists have been able to achieve in ceramic–matrix composites. Such impressive properties originate from the microstructural design possible by biological fabrication, essentially the organization of the biominerals and the protein matrix.

[a)]Address all correspondence to this author.
Present address: Department of Civil Engineering, University of Minnesota, Minneapolis, Minnesota 55455.
e-mail: broberto@umn.edu
DOI: 10.1557/JMR.2007.0016

From the morphology and organization of the biominerals, five common shell microarchitectures can be recognized in molluscan shells: the crossed-lamellar, nacreous, prismatic, foliated, and homogeneous microarchitectures.[4] The common characteristic of shell microstructures is that the building blocks are very small, with lengths of tens of nanometers to microns, and are organized in an ordered arrangement in at least one dimension.[5] The organic matrix is present as a thin envelope or sheet surrounding each mineral unit.[5] The mechanical properties of shells with different structures vary considerably.[2,6]

The crossed-lamellar microstructure is the most common structure in molluscan shells, represented in ~90% of gastropods and ~60% of bivalves, and is considered to be at the pinnacle of molluscan evolution. This structure, which exhibits the highest fracture toughness among the various shell microarchitectures, will now be described in detail to illustrate the hierarchical nature of molluscan shells. The mineral phase is generally aragonite (although there are a few examples of calcitic crossed-lamellar structures), whose morphology is approximately rectangular or lathe-like. As illustrated through the schematic diagram shown in Fig. 1, structure is present in the lamellar microarchitecture at five different length scales: the macroscopic layers; the first-, second-, and third-order lamellae; and twins within each third-order lamella. In Fig. 1, we note in particular that the middle layer (labeled M) is composed of parallel rows of first-order lamellae. The first-order lamellae in turn are composed of parallel rows of second-order lamellae, and in alternating first-order lamellae, the second-order lamellae are rotated by ~90°. Also, the first-order lamellae in the middle layer are oriented ~90° to the first-order lamellae in the inner and outer layers (labeled I and O, respectively, in Fig. 1). Shells with the crossed-lamellar structure contain only ~1% organic material, which is distributed at the interfaces between first-, second, and third-order lamellae.

Shell specimens of this type have an elastic modulus on the order of 50 GPa, moderately high bend strengths up to 100 MPa, and an extraordinarily high work of fracture up to ~13×10^3 J/m^2 (compared to the fracture surface energy of ~1 J/m^2 for nonbiogenic $CaCO_3$).[2,3,7,8] The impressive work of fracture, defined as the area under the load–displacement curve divided by the fracture surface area, is achieved through two energy-dissipating mechanisms that (as discussed below) are strongly influenced by the mechanical behavior of the organic phase. As the shell is subjected to mechanical bending loads producing tensile stresses in the outer layer, multiple tunnel cracks develop along first-order interfaces [shown schematically in Fig. 2(a)] at low loads but are arrested by the tougher middle layer. The mutual shielding produced by the interaction of these closely spaced interfacial cracks contributes to increased strength and ultimate strain to failure, and in turn a high work of fracture. Energetic arguments[9] revealed that for multiple cracks to develop, the ratio of nominal fracture toughness of the middle layer to that of the inner and outer layers must be greater than 2. This criterion was verified experimentally by Kamat et al.[3] in shells of *Strombus gigas*, whose measured toughness ratio of ~4 produces a 20-fold increase in the work of fracture, compared to the work of fracture of a geometrically similar specimen with a uniform toughness equal to that of the middle layer.

As the load is increased, a saturation tunnel crack density is eventually reached, and one or more of the cracks start to grow through the middle layer, along the interfaces between second-order lamellae. These cracks do not propagate catastrophically through the middle layer; instead they are retarded by the bridging action of the first-order lamellae [Fig. 2(b)]. The crack-bridging mechanism, which is similar to that observed in ceramic–matrix composites, enables the graceful failure of the shell and as a result, a work of fracture two orders of magnitude higher than the work of fracture of nonbiogenic aragonite.[10] In fact, Kamat et al.[10] have demonstrated that the shell's design is associated with intrinsic material length scales that enable it to approach the so-called Aveston–Cooper–Kelly limit,[11] a desirable situation in which the crack bridging ligaments remain intact as cracks traverse the specimen. Kamat et al.[10] also demonstrated, through four-point bend tests in a

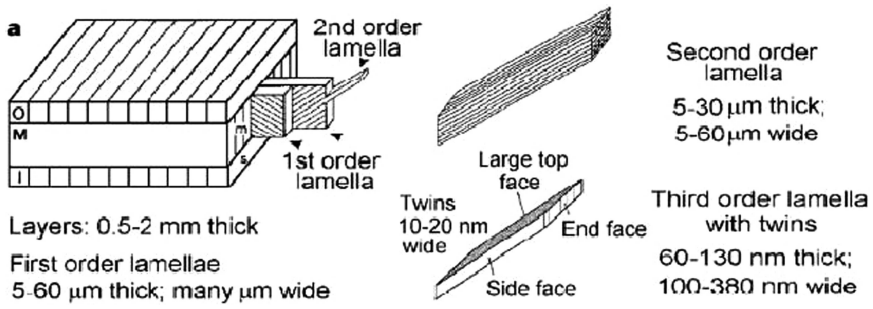

FIG. 1. Schematic illustration of the crossed lamellar microstructure of the shell of *Strombus gigas* (O, M, and I refer to outer, middle, and inner layers, respectively).

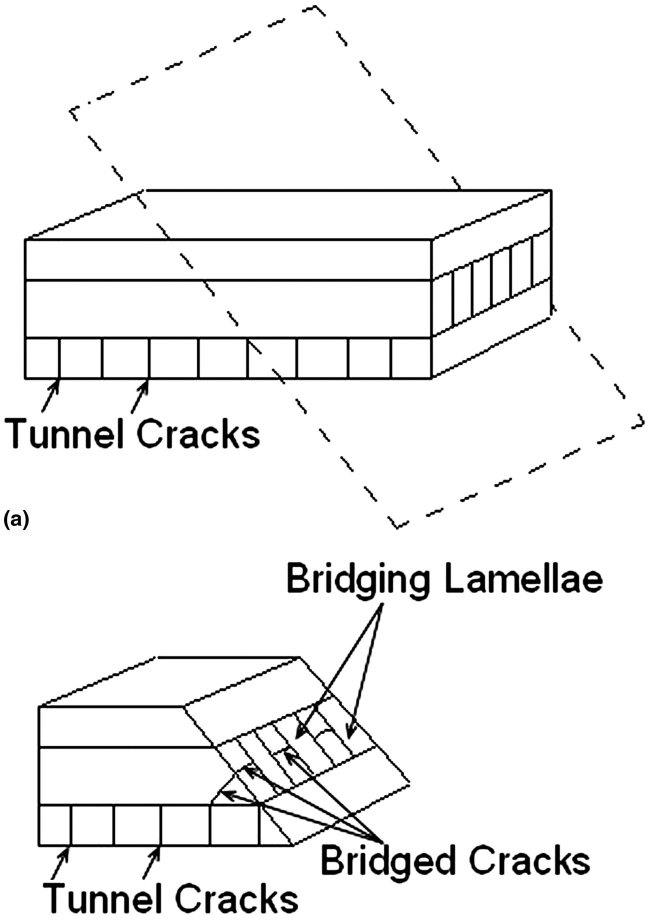

FIG. 2. (a) Tunnel cracks in the inner layer under low loads. (b) Bridged cracks propagating in the middle layer along the interfaces between second-order lamellae under high loads.

temperature-controlled chamber at temperatures ranging from –120 to 200 °C, that the role of the organic phase in the fracture resistance of the shell cannot be overstated. Their experimental results showed an increasingly brittle response at low temperature, as evidenced by relatively smooth fracture surfaces (suggesting the lack of fiber pullout that is responsible for crack-surface bridging), and in turn a lack of deformation in the post-peak region of the load–displacement curve. This embrittlement was attributed to a reduction in the resilience and damping characteristics of the organic phase and is consistent with the observations made in previous studies of the deformation characteristics of proteins in mollusks.[8,12,13] In particular, Smith et al.[13] used an atomic force microscope to stretch the organic molecules exposed on the surface of freshly cleaved nacre. The force–displacement response showed that these molecules deform in a step-wise manner as folded domains are pulled open and suggest that the organic matrix in mollusks is very specific. These experiments suggest that processing truly bioinspired composite structures may require procedures that introduce interphases that can experience very large and energy dissipating deformations. As explained below, we have made no attempt to do so or to determine whether the interphase we introduced into our composite structures is associated with what Smith et al. refer to as "modular" elongation.

In the past, organic–inorganic biomimetic composites have been constructed using self-assembly[14–16] or layer-by-layer[17,18] techniques. In this work, we used MEMS technology to fabricate a micro-composite that replicates the crossed-lamellar architecture of molluscan shells such as *Strombus gigas* in an attempt to reproduce tunnel cracks and crack bridging. The advantages of MEMS technology include the use of photolithography to achieve extremely ordered designs, such as that shown in Fig. 1. Also, length scales on the order of microns can be routinely realized.

II. EXPERIMENTAL

A. Design

For the bioinspired micro-composite, we chose silicon and photoresist to take on the roles of the (brittle and relatively strong) aragonite and the (tough and relatively weak) organic matrix. Silicon, the workhorse structural material in the integrated circuit (IC) and MEMS industries, is associated with mature microfabrication methods, and photoresist, a relatively tough polymer, is widely used in the same industries for transferring features from photomasks to silicon wafers. While the polymeric photoresist that we used in this study is expected to be less brittle than the silicon, we do not pretend that it is capable of creating strong bonding with the silicon or developing the large deformations and energy dissipation observed in the experiments of Smith et al.[13] This study is meant to be a proof of concept limited to specific materials combination and structural dimensions.

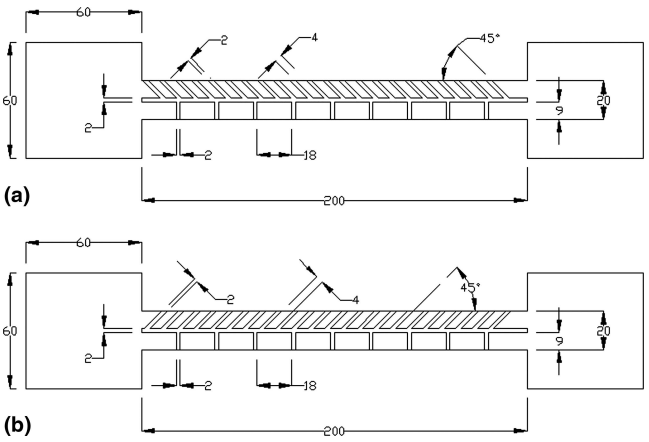

FIG. 3. Top view of designed structural geometry: (a) first and third film in three-film stack and (b) second film in three-film stack. Dimensions are in micrometers.

The laminated micro-composite is a doubly clamped beam that consists of a stack of three consecutively deposited films, two of which are shown schematically in Fig. 3. The architecture of each film is a two-length scale approximation of the inner (or equivalently outer) and middle layers of the shell of *Strombus gigas*. The inner layer (the bottom half of the beams sketched in Fig. 3) contains vertical interfaces whose role is to crack at relatively low loads, while the middle layer (the top half of the beams sketched in Fig. 3) contains interfaces oriented at either +45° or −45° with respect to the horizontal. The films are stacked with an alternating arrangement of the angled interfaces, so that in principle, the middle layer should be tough enough to arrest the tunnel cracks that develop in the inner layer. We have not yet fabricated structures with a larger number of layers and therefore do not know how sensitive the mechanical behavior is to the number of layers. We do note, however, that Kamat et al.'s study suggests that it is the three dimensional gradation of properties that enables biological structures to achieve superior mechanical performance.

The structural configuration is achieved by repeating the deposition of a thin silicon film three times to create the first structural layer, followed by the use of reactive ion etching (RIE) to dig the trenches that in turn are filled with photoresist. The 2-μm thickness of the interfaces corresponds to photolithography resolution limitations in the Case "fab" available to us, and renders the volume fraction of "organic matrix" higher than might be desired

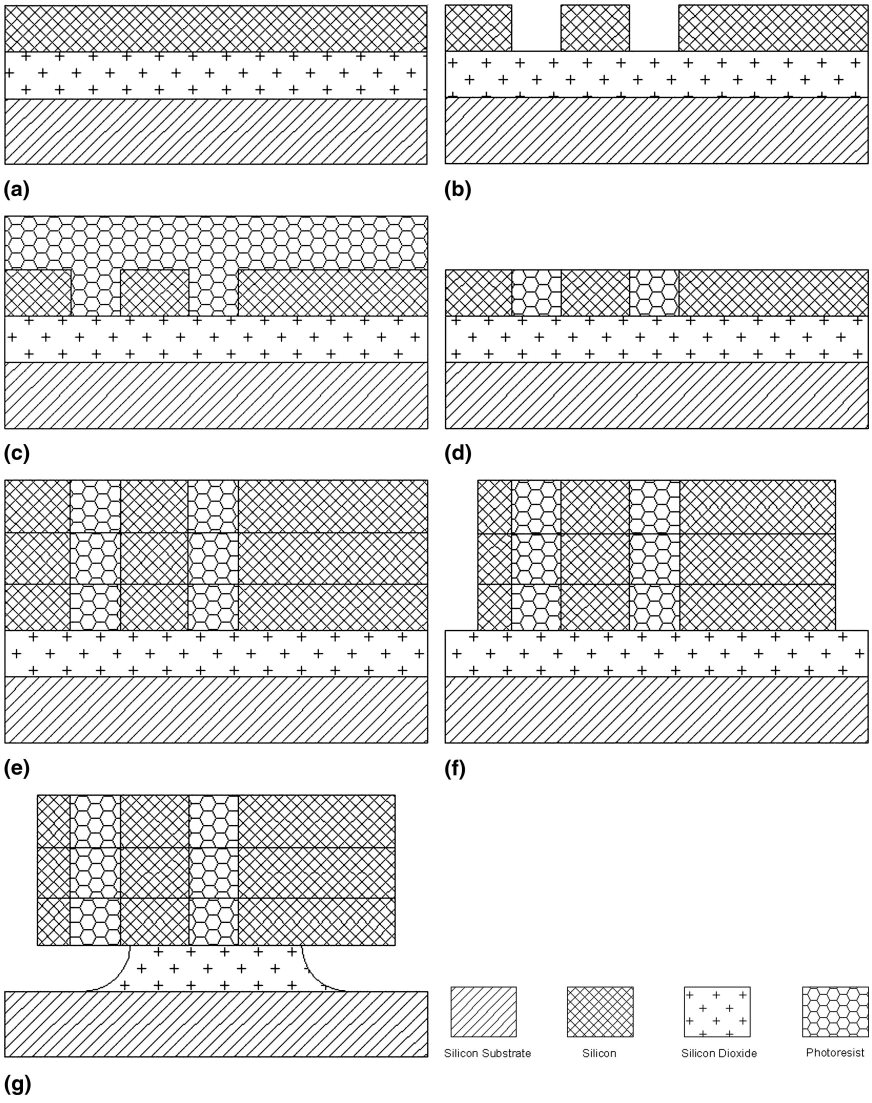

FIG. 4. Sketches of the fabrication design. Hatch labels indicate silicon is either amorphous or polycrystalline. (a) Deposit first layer silicon on the top of silicon dioxide film. (b) Etch trenches in the first layer silicon to form interfaces using RIE. (c) Apply photoresist on the top of the etched first layer silicon to fill the trenches. (d) Etch the photoresist on the top of the first layer silicon with RIE. (e) Repeat (a–d) twice to form a three-layer structure. (f) Etch the three silicon layers down to the silicon dioxide layer to form the specimen shape. (g) Release the specimen using BOE to etch silicon dioxide film.

for structural optimization. The fabrication sequence is shown in Fig. 4 and is discussed in the next section.

B. Fabrication

Two steps are critical for producing a structurally sound micro-composite: trench etching of the silicon layers and filling of the trenches with photoresist. The fabrication recipe is summarized next. More details can be found elsewhere.[19]

One-hundred-millimeter-diameter, 500-μm-thick silicon wafers were used. First, a 2-μm-thick silicon dioxide layer was thermally grown. After oxidation, a 2.5-μm-thick polysilicon film was deposited via low-pressure chemical-vapor deposition at 617 °C using SiH_4 gas with a deposition rate of 9.5 nm/min [Fig. 4(a)]. This polycrystalline film is associated with high compressive stress and was therefore annealed for 1 h at 1100 °C to reduce these residual stresses.

Standard photolithography was used to define the trenches in the first polysilicon layer using a LAM490 tool (Lam Research Corp., Fremont, CA), as shown in Fig. 4(b). Shipley 1813 photoresist (Phoenix, AZ) was spun on to fill in the trenches [Fig. 4(c)], and the photoresist left on top of the silicon film was removed [Fig. 4(d)]. The three-layer structure was achieved by repeating this procedure two more times [Fig. 4(e)] with slightly thinner sputtered silicon films (2.1 μm for the second film and 2.2 μm for the third film). A relatively thin layer of photoresist remained on the surface of the structure, as complete removal could potentially have led to damage to the third silicon film.

The 6.8-μm-thick structure was then etched using RIE to form the final structure [Fig. 4(f)]. After the final etching step, the wafer was dipped in a buffered oxide etch (BOE) solution containing HF for 155 min to completely release the devices [Fig. 4(g)]. Figure 5 shows a successfully released device.

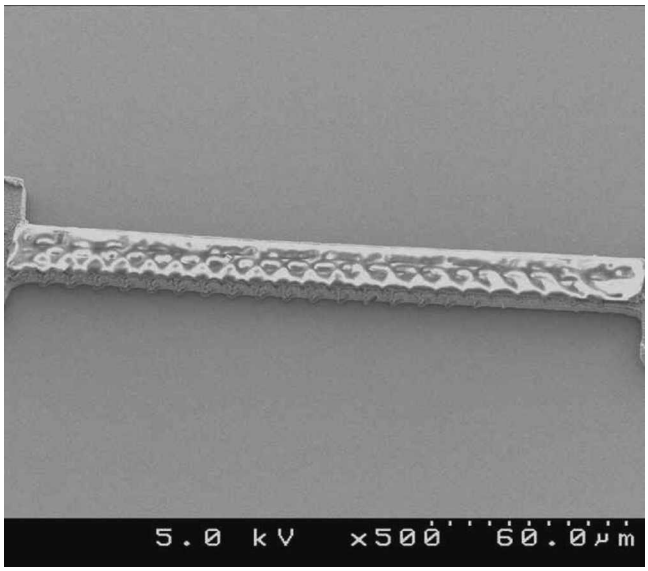

FIG. 5. SEM image of the released microstructure. The dimples are the photoresist that remains on the top surface.

C. Measuring the mechanical properties of the micro-composite

To test the mechanical properties of the MEMS fabricated micro-composite, the load–displacement behavior must be accurately measured when subjected to a lateral force. Because these parameters are on the order of micro-Newtons and micrometers, no standard mechanical testing equipment is available. Therefore, mechanical testing of the micro-composite was performed using a commercially available Triboscope nanoindenter (Hysitron, Inc., Minneapolis, MN) equipped with a lateral displacement transducer mounted on a Dimension 3100 scanning probe microscope (Veeco, Inc., Woodbury, NY). A schematic of the test is shown in Fig. 6(a). The load was applied through a custom fabricated punch with

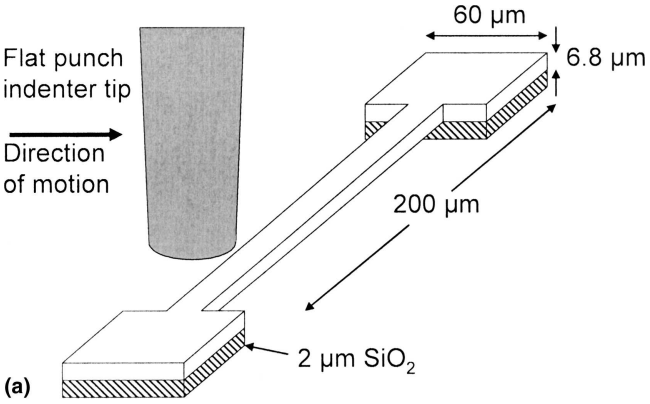

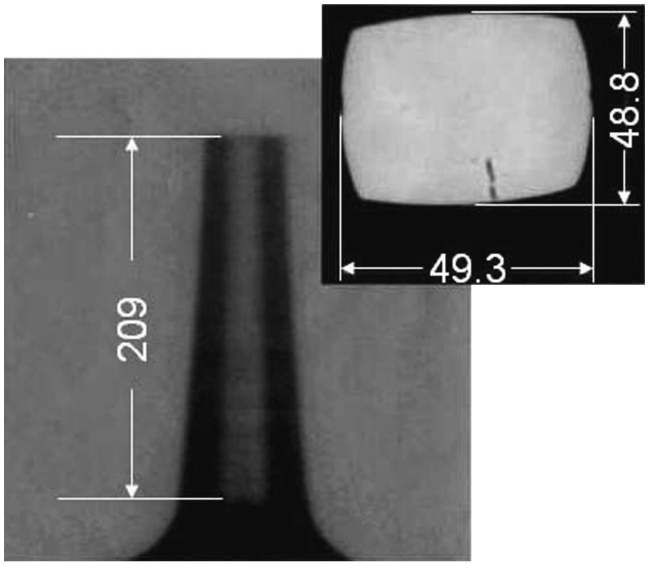

FIG. 6. (a) Schematic illustration of a mechanical test. (b) The side view of the flat punch tip and the top view of the tip free end; dimensions are shown in micrometers (images courtesy Hysitron, Inc.).

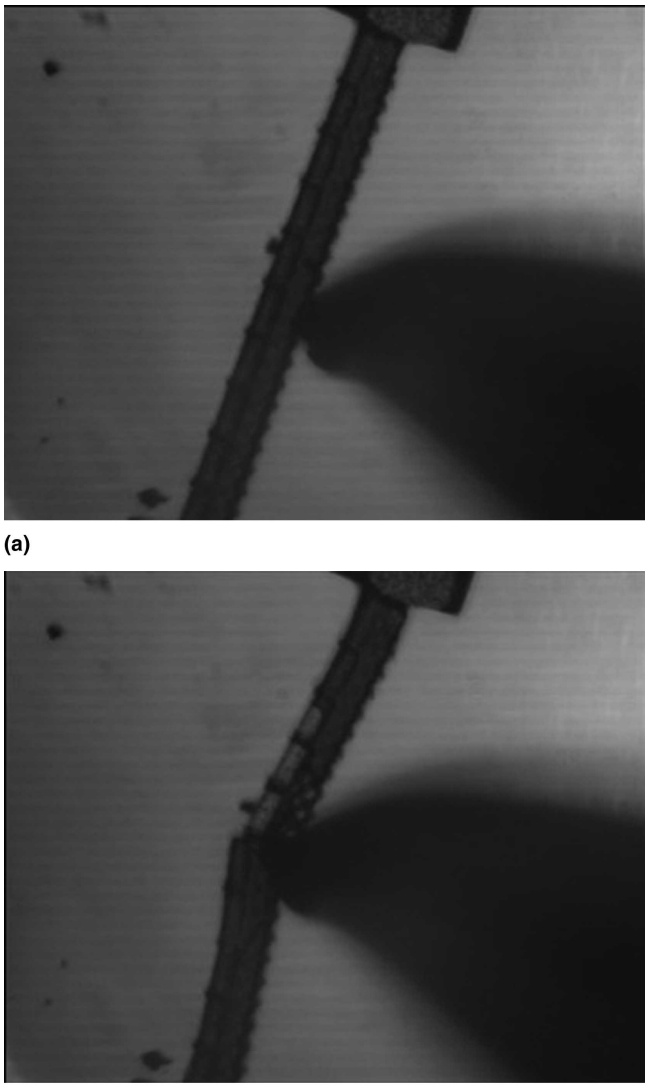

FIG. 7. (a) Microprobe position before pushing the beam. (b) Microprobe position after a catastrophic failure.

a flat tip whose side and cross-sectional views are shown in Fig. 6(b). The flat surface of the tip enabled mated contact with the substrate and mitigated the riding of the punch over the thin specimen. Specific data points in the load–displacement curve could not be associated with damage events because of the lack of an in situ high-magnification visual system to observe deformation history during loading.

The lateral (in-plane) test was conducted using displacement control at a stroke rate of 22 μm/min. No normal force was applied, and the vertical displacement and force were constantly monitored to ensure that the indenter tip did not ride over the specimens. The main disadvantage of the nanoindenter with the lateral force transducer was that the maximum stroke was limited to 10 μm. This proved to be insufficient to completely fracture the micro-composite beams. To determine the lateral deflection required for catastrophic failure, a micro-manipulated probe (with no force measurement) was used to fracture the micro-composite beams under an optical microscope (Fig. 7).

III. RESULTS AND DISCUSSION

Figure 8 shows two load–displacement curves typical of the 11 beams tested. While the limit of purely elastic deformation was abrupt, the ultimate load is significantly higher than the load required for initial damage. We again note that the beams did not completely fracture; the drop in force with slight negative displacement at the end of the test corresponds to the indenter tip returning to its original position. No attempt is made in this paper to explain the data using theoretical micromechanical models. Instead, the data are presented in terms of nominal

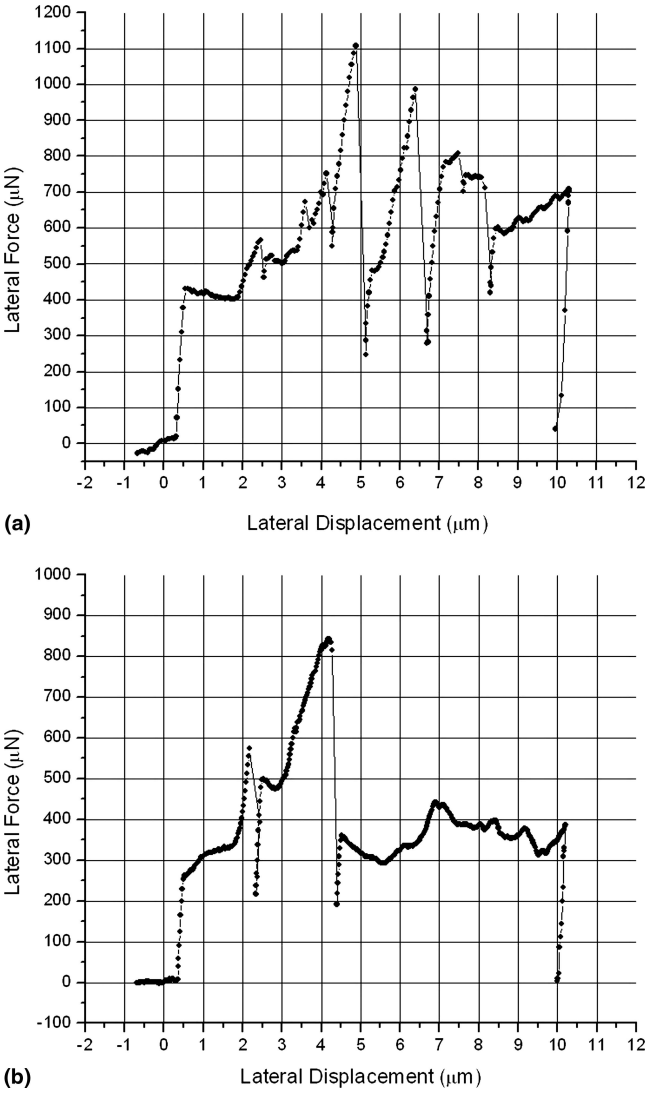

FIG. 8. Typical lateral load–displacement curves.

strength and dissipated energy. The 11 tests produced an average nominal yield stress of 11.4 MPa with a standard deviation of 3.1 MPa and an average ultimate strength of 26.3 MPa with a standard deviation of 4.2 MPa. These values correspond to those of a homogeneous doubly clamped elastic beam subjected to a point load with no axial forces, whose maximum stress is thus given as

$$\sigma = \frac{M\mathrm{d}}{I} = \frac{PLd}{8I} \quad , \tag{1}$$

where P is the applied (concentrated) load, L is the span of the beam, d is the half beam width, and I is its moment of inertia. For the micro-composite, the total beam thickness was measured using a Dektak profilometer (Veeco Instruments, Woodbury, NY), and the width was measured in the scanning electron microscope (SEM). The ultimate strength is approximately one fourth that of the shell of *Strombus gigas*.

Figure 9(a) is a SEM image of a (loaded and then unloaded) specimen, taken from a vantage point directed towards the side of the outer layer. Only one tunnel crack is observed, suggesting that the ratio of fracture toughness of the middle layer to the outer layers is not sufficiently high to create multiple tunnel cracking.[9] However, another specimen viewed from the opposite side [Fig. 9(b)] indicates a significant amount of other energy dissipating cracking events, such as delamination between the three stacks, and bridged cracks along the ±45° interfaces.

The toughness of the micro-composite was quantifed, as measured by the work required by the load to fracture the specimen into two pieces. As discussed above, the maximum lateral stroke of the nanoindenter was insufficient to completely fracture the micro-composite beams. By videotaping six beams as they were pushed to failure with a micro-probe (Fig. 7), the maximum displacement was found to be 16 ± 1 μm. Therefore, the following values obtained for the dissipated energy in each micro-composite are lower bounds, since they do not account for any energy dissipation in the final ~6 μm of deflection. We are currently making modifications to the test setup that will enable us to capture the complete load–deflection curve.

The total energy dissipated by each specimen $E_{\mathrm{composite}}$ was calculated by integrating the area under the load–displacement curve. The average $E_{\mathrm{composite}}$ is 4900 ± 1200 μN μm.

The dissipated energy is compared to that associated with the cracking of a monolithic piece of silicon E_{Si} into two pieces. The piece is obtained by multiplying an assumed surface energy $2\gamma = 1$ J/m^2 by the cross-sectional area of the beam, providing a fracture resistance equal to 136 μN μm. Thus, a first measure of increased toughening is provided by the ratio $E_{\mathrm{composite}}/E_{\mathrm{Si}} = 36$.

Another measure of the graceful failure of the micro-composite is the brittleness index B, defined as

$$B = \frac{A_{\mathrm{E}}}{A_{\mathrm{postpeak}}} \quad , \tag{2}$$

where A_{E} is the area under the elastic part of the load–displacement curve (the elastic strain energy) and A_{postpeak} is the area in the post-peak region of the force–displacement curve. For monolithic sputtered silicon, the only energy dissipation is the energy of the newly created fracture surfaces, so that the $B = \infty$. For the fabricated microstructure, $B = 0.010 \pm 0.002$, a very small number implying that the fabricated microstructure exhibits significant ductility.

While both the micro-composite studied in this work and the *Strombus gigas* shell[10] displayed significant toughness and ductility compared to monolithic silicon or aragonite, there were differences in the specific

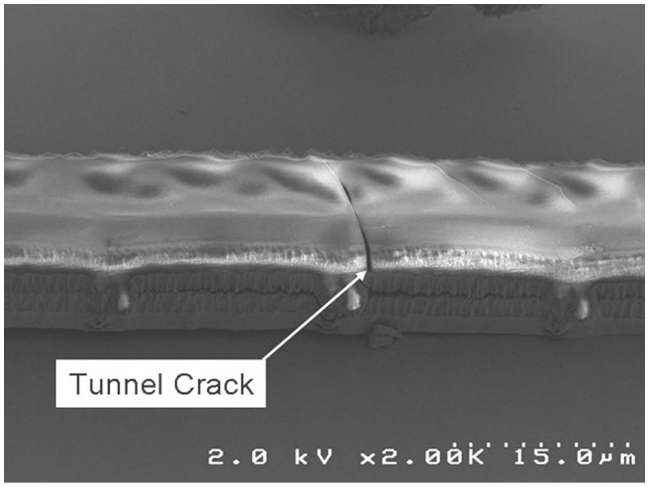

(a)

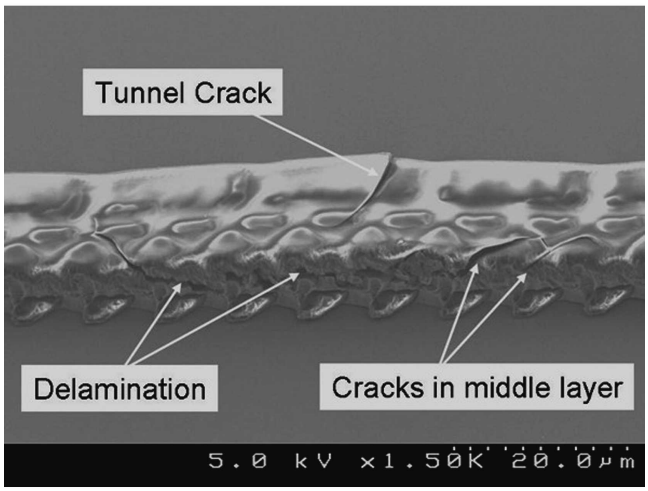

(b)

FIG 9. SEM images of two tested beams: (a) inner layer side view and (b) middle layer side view.

energy-dissipating mechanisms. In particular, the mollusk shell displayed multiple tunnel cracking and bridged cracks, and the micro-composite displayed delamination and bridged cracks. These differences could have been caused by the excessive thickness of the photoresist layers in the micro-composite (2 μm), compared to the thickness of the protein matrix in the mollusk shell (~10–300 nm).[3]

IV. CONCLUSIONS

An innovative micro-fabrication procedure was developed for making a three-dimensional laminated bioinspired micro-composite structure composed of brittle and ductile components. In particular, photoresist, which is normally used as an etching mask, was used as a structural component, along with silicon.

While the bioinspired microarchitecture, which mimics the crossed-lamellar structure found in mollusks, did not produce as much multiple tunnel cracking as observed in mollusk shells, several energy-dissipating cracking patterns such as delamination and bridged cracks did develop, and a significant strength and work of fracture was achieved. This work is an "existence proof" of the power of MEMS-based fabrication procedures for bioinspired design of structural composites.

ACKNOWLEDGMENTS

Financial support from the National Science Foundation (Grant No. CMS-0226373) is gratefully acknowledged. The authors thank Dr. Kimberly Turner of University of California Santa Barbara for making her nanoindentation equipment available to us in the early stage of this research.

REFERENCES

1. J.D. Currey and J.D. Taylor: The mechanical behavior of some molluscan hard tissues. *J. Zool.* **173,** 395 (1974).
2. L.T. Kuhn-Spearing, H. Kessler, E. Chateau, R. Ballarini, and A.H. Heuer: Fracture mechanisms of the *Strombus gigas* conch shell: Implications for the design of brittle laminates. *J. Mater. Sci.* **31,** 6583 (1996).
3. S. Kamat, X. Su, R. Ballarini, and A.H. Heuer: Structural basis for the fracture toughness of the shell of the conch *Strombus gigas. Nature* **405,** 1036 (2000).
4. O.B. Bøggild: The shell structure of the molluscs. *K. Danske Vidensk. Selsk. Skr.* **2,** 232 (1930).
5. C. Gregoire: Structure of molluscan shell, in *Chemical Zoology,* edited by M. Florkin and B.T. Scheer (Academic Press, New York, 1972), p. 45.
6. A.P. Jackson, J.F.V. Vincent, and R.M. Turner: The mechanical design of nacre. *Proc. R. Soc. London Ser. B* **234**, 415 (1988).
7. V.J. Laraia and A.H. Heuer: Novel composite microstructure and mechanical-behavior of mollusc shell. *J. Am. Ceram. Soc.* **72,** 2177 (1989).
8. A.P. Jackson, J.F.V. Vincent, and R.M. Turner: Comparison of nacre with other ceramic composites. *J. Mater. Sci.* **25,** 3173 (1990).
9. H. Kessler, R. Ballarini, R.L. Mullen, L.T. Kuhn, and A.H. Heuer: A biomimetic example of brittle toughening: (I) Steady state multiple cracking. *Comp. Mater. Sci.* **5,** 157 (1996).
10. S. Kamat, H. Kessler, R. Ballarini, M. Nassirou, and A.H. Heuer: Fracture mechanisms of the Strombus gigas conch shell—(II) Micromechanics analyses of multiple cracking and large-scale crack bridging. *Acta Mater.* **52,** 2395 (2004).
11. J. Aveston, G.A. Cooper, and A. Kelly: Properties of fiber composites, in *Conf. Proc. 15* (National Physical Laboratory, IPC Science and Technology Press, Guilford, Surrey, UK, 1971).
12. *Elastomeric Proteins: Structures, Biomechanical Properties, and Biological Roles,* edited by P.R. Shewry, A.S. Tatham, and A.J. Bailey (Cambridge University Press, 2003).
13. B.L. Smith, T.E. Schäffer, M. Viani, J.B. Thompson, N.A. Frederick, J. Kindt, A. Belcher, G.D. Stuckey, D.E. Morse, and P.K. Hansma: Molecular mechanistic origin of the toughness of natural adhesives, fibres and composites. *Nature* **399,** 761 (1999).
14. H. Cölfen and S. Mann: Higher-order organization by mesoscale self-assembly and transformation of hybrid nanostructures. *Angew. Chem., Int. Ed. Engl.* **42,** 2350 (2003).
15. J. O'Kelly, R. Crockett, H. Martin, and P. Calvert: Biomimetic processing of gel glasses and organic-inorganic hybrids. *J. Sol.-Gel Sci. Technol.* **8,** 641 (1997).
16. C. Li and D.L. Kaplan: Biomimetic composites via molecular scale self-assembly and biomineralization. *Curr. Opin. Solid State Mater. Sci.* **7,** 265 (2003).
17. Z. Tang, N.A. Kotov, S. Magonov, and B. Ozturk: Nanostructured artificial nacre. *Nat. Mater.* **2,** 413 (2003).
18. G. Mayer: Rigid biological systems as models for synthetic composites. *Science* **310,** 1144 (2005).
19. L. Chen: A bioinspired micro-composite structure. Ph.D. Dissertation, Case Western Reserve University, Cleveland, OH (2005).